Chemical, morphological and mechanical study of the ageing of textile flax fibers from 17th/18th-century paintings on canvas

Alessia Melelli, Graziella Roselli, Noemi Proietti, Alain Bourmaud, Olivier Arnould, Frédéric Jamme, Johnny Beaugrand, Alice Migliori, Giuseppe Di Girolami, Paolo Cinaglia, et al.

CHEMICAL, MORPHOLOGICAL AND MECHANICAL STUDY OF THE AGEING OF TEXTILE FLAX FIBERS FROM 17th/18th-CENTURY PAINTINGS ON CANVAS

Alessia Melelli[a*], Graziella Roselli[b], Noemi Proietti[c], Alain Bourmaud[a], Olivier Arnould[d], Frédéric Jamme[e], Johnny Beaugrand[f], Alice Migliori[g], Giuseppe Di Girolami[g], Paolo Cinaglia[g], Carlo Santulli[h]

[a] Univ. Bretagne Sud, UMR CNRS 6027, IRDL, F-56100 Lorient, France

[b] School of Sciences and Technologies (SST), Università di Camerino, Chemistry Division, via S.Agostino n.1, 62032 Camerino, Italy

[c] Laboratorio di Risonanza Magnetica "Capitani-Segre", Istituto per i Sistemi Biologici, Area della ricerca di Roma 1, CNR, 00015 Monterotondo, Roma, Italy

[d] LMGC, Université de Montpellier, CNRS, Montpellier, France

[e] Synchrotron SOLEIL, DISCO beamline, Gif-sur-Yvette, France

[f] UR1268 Biopolymères Interactions Assemblages, INRAE, Nantes, France

[g] Università di Camerino, Innovative Techniques for Cultural Heritage, via Pacifici n.2, Ascoli Piceno, 63100 Italy

[h] School of Sciences and Technologies (SST), Università di Camerino, Geology Division, via Gentile III da Varano, 62032 Camerino, Italy

*Corresponding author: alessia.melelli@univ-ubs.fr;

Institut de Recherche Dupuy de Lôme
UMR CNRS 6027
Centre de recherche Huygens
Rue de Saint-Maudé
BP 92116-F-56321 Lorient cedex, France

Length of the manuscript (with references): 7525 words

Length of the manuscript (without references): 5437 words

Abstract

A variety of techniques were used to investigate flax yarns sampled from four selected Italian paintings on canvas dated between the 17th and 18th centuries and compare them with a modern flax yarn. The goal was to establish their state of preservation and highlight the critical issues thanks to a combined approach that used SEM, atomic force microscopy, nanoindentation, nuclear magnetic resonance, second harmonic generation imaging microscopy and FTIR spectroscopy. The condition of the flax fibres was assessed, and the results showed that two of the four canvases were in a generally good state of preservation, while the other two exhibited signs of biological attack and brittleness due to a previous re-lining intervention.

Keywords: paintings on canvas; flax fibres; degradation; cellulose modification; mechanical properties

1. Introduction

Flax (*Linum Usitatissimum* L.) is one of the oldest domesticated plants [1], used for its fibres and, in the food sector, for its seeds. In Europe, starting from the Late Middle Age, a number of plant fibres, such as hemp and flax, have played a key role as a support for paintings on canvas, especially flax for its great homogeneity and fineness coupled with excellent mechanical properties, suitable to face the stresses and deformations that paintings undergo.

One of the methods used by artists to prepare the textile support before painting is reported in Cennino Cennini's treatise, dated to circa 1400 [2]. However, each artist had his own method and used materials of different qualities often linked to his social rank

and his clientele [3], though common characteristics can be found by geographical area and historical period [4].

In general, the textile layer of a canvas has the function of supporting several other layers of different natures, since pigments are not applied directly on it. For centuries, the first layer was composed of glue, usually of animal origin, as also mentioned in Cennini's treatise [1], followed by the ground layer (gypsum or calcium carbonate and glue or flour, oil and pigments), but around the 17th century, the first layer of glue, in contact with the textile support, was sometimes omitted because artists tried to preserve the *recto* of the canvas support from humidity [4]. Currently, it is known that animal glue promotes the growth of mould and bacteria [3,5].

Several studies have focused their attention on the mechanical properties of textile supports by measuring the vibrations or tension of canvases [6–9]. Two important methods to evaluate the state of preservation of the textile support are the calculation of the degree of polymerisation (DP) of cellulose (by viscometry or GPC) [10] and the determination of the cellulose morphology and microstructural heterogeneities with solid-state nuclear magnetic resonance spectroscopy (^{13}C CP-MAS NMR). In particular, the last technique only requires small amounts of material, namely 25 µL [11,12], which corresponds to approximately 30 mg of sample. Due to the small amount of sample usually available from cultural objects such as paintings, a combination of techniques is usually necessary to have a clear evaluation of the state of preservation of artworks.

For example, scanning electron microscopy (SEM) or optical microscopy have been combined with techniques capable of obtaining information on cellulose crystallinity and chemical modifications, such as X-ray diffraction (XRD), Fourier transform infrared (FTIR) or Raman spectroscopy [13–15].

Furthermore, other techniques generally used in the engineering and biology fields can also be employed for the study of cultural heritage, especially regarding the study of cellulosic fibres, such as atomic force microscopy (AFM) and nanoindentation, which allow us to investigate the micromechanical properties of the cell walls [16], and second harmonic generation imaging (SHG) [17,18], which offers data on the fibre, especially cellulose ultrastructure.

This work aims to establish the state of preservation of four Italian canvases dated between the 17th and 18th centuries and to elucidate possible degradation using a new combination of techniques that thus far has found very limited application in the conservation field. The canvases were first imaged by optical and scanning electron microscopy to obtain information on their morphology. Successively, local mechanical properties were examined by nanoindentation and AFM techniques, while chemical information was obtained by FTIR-ATR spectroscopy and NMR to obtain an overview of the state of preservation of each canvas. Finally, SHG microscopy was used to assess the state of the fibre ultrastructure.

2. Research aims

The aim of this research was to establish the state of preservation of four paintings on canvas displayed at the Civic Art Gallery of Ascoli Piceno based on data acquired by a new combination of techniques, i.e., atomic force microscopy, second harmonic generation imaging microscopy, FTIR spectroscopy, SEM and ^{13}C CP-MAS NMR. Our results can help curators recognise canvases in the worst condition that require immediate intervention or more in-depth investigation by conservators; at the same time,

this new pairing of techniques can support the study of other ancient artefacts made of plant fibres, such as clothing and tapestries.

3. Experimental

3.1. Samples

Yarns from four oil paintings dated between the 17th and 18th centuries were examined. The paintings are currently stored at the Civic Art Gallery of Ascoli Piceno. Details about the paintings are given in Table 1. Yarn samples were taken from the *recto* of each canvas in excess areas beyond the mounting frame to avoid, as much as possible, the ground and paint layers. The sample amount taken from each painting was on the order of 50 mg.

A contemporary yarn was used as a reference sample. It was produced from textile flax (Melina variety) cultivated in 2018 in Normandy (France) by the Teillage Saint-Martin company; this flax was dew-retted conventionally over 6 weeks and then scutched and hackled. Then, it was wet spun by Safilin Pionki (Poland) with a metric number of 9.7 km/kg and a targeted twist of 320 tpm.

Table 1.

3.2. Experimental methods

Several microscopic and spectroscopic techniques were applied and briefly described in Table 2, which summarises the setup and parameters chosen for the analysis.

3.2.1 Scanning Electron Microscopy (SEM)

To examine the fibre surface morphology, a small piece of yarn approximately 5 mm long was cut from each sample, and the modern yarn was adhered to a conductive sample holder and successively gold sputter-coated (Edwards Scancoat Six device for 180 seconds) to perform SEM micrographs.

3.2.2 Atomic force microscopy (AFM) and nanoindentation

In AFM, a laser beam is focused on a tip mounted on a cantilever, and the laser reflection is recorded by a photodetector. The deflection of the cantilever by the tip-sample interaction can be converted into a force-distance curve when the tip indents the surface. The peak force quantitative nanomechanical property mapping mode (PF-QNM) is based on the recording of force-distance curves at a high rate (2 kHz) for a limited maximum load (200 nN in this paper) and thus a limited indentation depth (on the order of a nanometre) while the tip scans the surface of the sample. The local indentation modulus is extracted from the unloading curve using a DMT model. This provides a map of indentation moduli in a few tens of minutes for a surface of several square micrometres, giving information on local mechanical properties of the cell walls, which are linked with the state of preservation of artworks. To the best of our knowledge, no literature exists regarding the use of AFM PF-QNM to investigate archaeological objects. Conversely, nanoindentation (NI) measurements are more widespread and are done with a deeper (i.e., several tens of nanometres up to more than a hundred nanometres) indent than AFM (i.e., indentation depth of a few nanometres here). Thus, the minimum spatial distance between two measurement points is much smaller in AFM than in NI. NI thus leads to a lower spatial resolution than that of AFM but, on the other hand, it allows to

obtain more qualitative and accurate mechanical properties. NI has already been used to investigate cultural artefacts [19,20], although the available literature is still scarce.

To prepare the samples for AFM analysis, a small piece of yarn approximately 5 mm long was cut from each canvas and embedded in low viscosity epoxy resin kit from Agar scientific (UK). The blocks prepared were put in an oven overnight at 60 °C, and their surface was successively cut using an ultramicrotome (Ultracut S, Leica Microsystems) equipped with diamond knives (Histo and Ultra AFM, Diatome). Sapphire was used to calibrate the deflection sensitivity of the AFM, the cantilever stiffness was calibrated using the Sader method, and a relative method was chosen to calibrate the tip radius using Aramid fibres K305 Kevlar 21 Taffetas 305 g/m² (Sicomin epoxy systems-France) as standard material [16]. At least four AFM images were obtained from each sample and the modern yarn. An averaged indentation modulus was calculated as a mean of the pixels included in the region of interest manually delimited by a mask, as shown in Figure A.1. Successively, a further average was calculated using the values obtained from the various figures of each yarn.

Nanoindentation measurements of the indentation modulus and hardness were performed on the same blocks of epoxy resin with embedded yarns previously prepared for AFM analysis. At least 30 points were tested for each yarn embedded in epoxy resin and representative of each canvas investigated, except for yarn TS1: here, 16 points were tested because the block had a lower number of fibres embedded and had a smaller diameter. In addition, approximately 20 points were recorded in the epoxy embedding resin of each block to check the stability of the measurements. The obtained indentation moduli were compared to the average calculated by AFM: in practice, the averaged AFM results were validated by nanoindentation, which operates at a higher scale.

3.2.3. Second harmonic generation microscopic imaging

Second harmonic generation (SHG) is a coherent nonlinear optical process in which two photons interacting with a medium are upconverted to a single photon with twice the incident frequency, and the phenomenon is generated by noncentrosymmetric molecules, such as cellulose. SHG microscopy is plane selective, and different levels in the Z-direction can be analysed independently from one another and allow us to investigate the inner structure of the samples, such as the angle formed by cellulose microfibrils in plant fibres [17,18]. For SHG analysis, a small bundle of each yarn was manually extracted and mounted on a paper frame used for traction tests according to technical standard ASTM C1557 [21]. This standard explains the preparation, mounting and testing of elementary fibres to determine tensile strength and Young's modulus; the sample support described in the technical standard is illustrated in Melelli et al. [18].

In this paper, the ancient yarns were glued in the standard support but in the transverse direction to use a 5 mm gauge length instead of 10 mm, successively placed between two coverslips and studied with a multiphoton microscope.

3.2.4. Solid-State ^{13}C CP-MAS NMR Spectroscopy

^{13}C cross-polarisation magic angle spinning NMR spectroscopy is an NMR technique that allows samples to be studied directly in the solid-state without having to dissolve them in a suitable solvent. This allows the study of small fragments of the object and their subsequent reuse for other investigations. In addition, the rotation around the angle defined as the "magic angle" allows sharpening of the resonance lines that, in the case of solid samples, are very wide.

^{13}C CP-MAS NMR spectroscopy has been used to investigate structural changes in cellulose-based materials, allowing the determination of the crystalline/amorphous ratio and the detection of hemicellulose, cellulose oligomers and noncellulosic compounds, such as organic additives.

Flax yarns were finely cut using a microcutter and packed into 4 mm zirconia rotors with an available volume set toto 25 µL and sealed with Kel-F caps. Cross-polarisation was achieved by applying the variable spin-lock sequence RAMP–CP-MAS [22]. Spectra were acquired using 1024 data points in the time domain, zero filled and Fourier transformed to a size of 4096 data points applying exponential multiplication with a line broadening of 16 Hz.

The deconvolution of ^{13}C CP-MAS spectra was performed using the dm2004 program [23], and the integrals of the resonances obtained from the deconvolution allow a semiquantitative evaluation. Each resonance was modelled by the following parameters: amplitude, position, width at half height and Gaussian line shape. Applying the best fitting procedure, the area and the chemical shift of all resonances were obtained. The sum of the integral of all resonances in each spectrum was normalised to 100. Fig. A.2 illustrates the details of the deconvolution of C1 and C4.

The crystallinity index (CI) of cellulose was calculated as a percentage of the integrals of the C-4 peaks at 86–92 ppm (C_{4c}) and 80–86 ppm (C_{4a}) [23]**:** $CI(\%) = 100\ C_{4c}/(C_{4c} + C_{4a})$. The resonance at approximately 106 ppm (C1 carbon) reveals the presence of I_α and I_β crystalline forms and can be used to evaluate the ratio $R = I_\alpha/I_\beta$, which depends on the source of the cellulose [12].

3.2.5. Fourier-Transform Infrared Spectroscopy (FTIR)

A linear baseline correction was performed using three points at 4000, 3700 and 1800 cm^{-1}. The spectra were rescaled, setting the minimum absorbance measured between 4000 and 1800 cm^{-1} to 0 and the maximum absorbance measured 1027 and 1002 cm^{-1} to 1.

Table 2

4. Results and Discussion

4.1. Morphological description of yarns and flax fibres

Thread count is an important parameter to characterise canvases and textile fabrics, and it plays an important role in the mechanical properties of the canvases [24,25]. All the canvases except TS1 had a plane weave structure (Figs. 1A, D, G, J), and GB appeared tauter than the others. GB and TS2 had similar thread counts (29/28 for the first one and 29/27 for the second one), and were coarser and more open-weave fabrics than NM (47/47) and TS1 (38/32), as shown in Fig. 1.

Figure. 1

For all the yarns investigated by SEM, the morphology indicated that they were flax fibres due to their polygonal shape (Fig. 1. C, F and I) and the presence of characteristic structural defects, i.e., kink-bands (Fig. 1. C, F, I and L). Generally, fibres appeared well separated, although residues of middle lamellae or cortical parenchyma sometimes remained glued to the fibre surface (Fig. 1. B), suggesting a possible subretting degree

for the GB sample. Nevertheless, the overall fibre separation was good, probably thanks to the retting mode, which in the past was carried out in water, as in ancient Egypt [26]. This method consists of soaking the fibres in water for approximately two weeks before scutching them, but since the second half of the 20th century, water retting has been replaced in Europe by dew retting, which produces less pollution, even if the quality of the fibre produced is lower [27].

In all the yarns, kink-bands were highly visible, especially on yarn NM, as shown in Fig. 1F. These defects are considered areas of weakness [28] and possible origins of fractures [29]. Other teams also observed that both enzymatic and acid hydrolysis start and act mainly in these regions [30,31] and can lead to fibre fragmentation. Thus, it can be assumed that cracks and porosities in kink-bands could facilitate the attack of microorganisms, which penetrate into the internal structure of the fibre to reach the lumen where they grow and then spread to the rest of the fibre cell [32].

Finally, in our samples, large residues were detected on yarn TS2, probably due to both ground layer (as indicated by SEM-EDX analysis, data not shown in this paper) and an adhesive from the past re-lining intervention (Table 1). During the 19th century, in Europe, the adhesive used for re-lining interventions was glue paste, a mix of animal glue, flours and Venice turpentine or other components [3,25].

The presence of this adhesive in yarn TS2 is particularly important in this case because today, it is known that glue paste can have dramatic consequences for paintings. It causes the canvas to have a greater susceptibility to humidity but also results in shrinkage and greater rigidity, and it is also highly sensitive to microbiological attack, especially in the case of animal glue [33–35].

An interesting study was recently performed by Fuster-López et al. in which the authors tested the glue paste on canvases and observed its ageing process [25]. They found

that, in aged samples, the glue paste appeared more crystallised, dryer and sometimes delaminated. Tensile test analysis showed that the canvases with aged glue paste were as sensitive to low relative humidity as the canvases treated with unaged glue paste. Fuster-López et al. also observed that the sensitivity to biodegradation, structural modification and the loss of mechanical properties were also dependent on the type of flour used in glue paste and the weave density of the linen canvas [25].

4.2. Investigation of local mechanical properties

Images obtained by AFM PF-QNM (Fig. 2) show that ancient fibres can have a stiffness similar to that of a modern flax, which is in general approximately 18–20 GPa [16,36] and in the present work measured approximately 19.4 ± 0.9 GPa by AFM and 20.7 ± 2.9 GPa by nanoindentation. However, in most cases, the indentation moduli obtained from ancient yarns are higher than those obtained from the modern yarn, clearly illustrated in the profile extracted from TS1 in Fig. 2. where the stiffness is calculated as approximately 24 GPa.

Despite their ageing, the flax fibres of ancient yarns still appeared homogeneous and had an intact structure (Fig. 2). Nevertheless, a high indentation modulus can be indicative of a chemical change due to ageing that occurs mainly in the cell wall matrix, as reported in [37]. It should also be pointed out that the flax fibres compared in the present work are neither from the same variety nor harvested at the same maturity or retted in the same manner. These differences play a central role in the mechanical properties and chemical composition of the fibres [38,39], and the results obtained must be regarded with caution.

Figure. 2

In general, the average data obtained by both AFM and nanoindentation techniques were in agreement (Fig. 3a). Yarn GB showed indentation moduli in line with those of the modern flax in both AFM (19.2 ± 3.3 GPa) and nanoindentation (19.3 ± 5.2 GPa) analyses. However, some flax fibres from this yarn showed fractures (see Fig. 3c), which were probably generated during the surface preparation by the diamond knife, and their appearance could be indicative of a higher brittleness than in the modern yarn.

In canvas NM, most of the fibres appeared intact with indentation moduli of approximately 20 GPa (20 ± 6 GPa by AFM and 17.5 ± 4.5 GPa by nanoindentation), but, in the bottom right of the map shown in Fig. 2, an extremely low indentation modulus (approximately 11 GPa) was recorded in one fibre, which indicates a great loss of local mechanical properties probably as a consequence of a chemical change not only in the matrix but also in the crystalline cellulose. This confirmed the suitability of the AFM technique to study aged yarns, as it is sensitive to the variable state of preservation of a canvas.

Fractures similar to those of the yarn GB were found in the yarn NM (Fig. 3c), for which the lowest hardness was also recorded (Fig. 3b).

Paintings TS1 and TS2 were painted for the abbot's lodging and were probably exposed to similar environmental conditions.

The highest indentation moduli were recorded in yarn TS1 (23.4 ± 3.4 GPa by AFM and 23.9 ± 5.4 GPa by nanoindentation), which could correspond to a change in the chemical composition of the hemicellulose matrix, as hypothesised in a previous study [37]. Some fibres of this yarn were fractured, such as yarn GB, but with signs of biological attack highlighted by a loss of mechanical properties (~ 11 GPa) around a cavity, as illustrated in Fig. 3c.

In terms of morphology, the best preserved fibres were found in yarn TS2, where no fractures were noted inside the cells (Fig. 2). However, this canvas underwent a past restoration intervention, and it was relined because of its poor state of preservation. In this last yarn investigated, the standard deviation of indentation moduli was comparable to that of the modern yarn (20.9 ± 3.9 GPa by AFM and 20.8 ± 3.7 GPa by nanoindentation), but the hardness is the highest recorded, probably because of a different ageing process of the cellulose matrix caused by the coating. A hypothesis could be that the exchange of water molecules and oxygen between the fibres and the environment was reduced by the coating, leading to a different ageing process of the cells than that found in the other canvases. As previously discussed, this canvas was relined, and traces of animal glue were found by FTIR and NMR (see Sections 4.3.1 and 4.3.2), while SEM analysis confirmed that the fibres of this canvas were coated. During the AFM analysis, some fragments were noticed on the fibre surface, probably due to the glue paste, as illustrated in Fig. 3c. The fragment did not cause visible changes to the mechanical properties of the fibres, which were still homogeneous in their indentation moduli, even in their external layers (primary and S1 cell walls).

Figure. 3

4.3 Chemical and structural modifications

4.3.1 FTIR results

Figure. 4

Table 3

The spectra and their attributions are reported in Fig. 4 and Table 3, respectively. Traces of gypsum (3525 and 3394 cm^{-1}) and calcite (874 and 713 cm^{-1}) were found in samples NM, TS1 and TS2 (Fig. 4a). The increase in the peak at 1735 cm^{-1} in spectra collected from the yarns of the canvases can be due to the oxidation process [40]. The band at 1595 cm^{-1} due to lignin [42,51] was noted only in the modern yarn. The absence of this peak in the canvas samples, together with the presence of the band at 2954 cm^{-1} (Fig. 4b), could suggest a form of lignin degradation.

Two bands at 1577 and 1540 cm^{-1} were particularly visible in yarn TS1 (Fig. 4b and Table 3), less visible in NM and probably also present in GB. These two bands are not documented in the literature for cotton or flax fibres and fabrics and are thus apparently not generated by the fibres. Zotti et al. observed them in ancient prints where fungal colonies were isolated, and the authors attributed these bands to a possible calcium stearate [53]. These two peaks can be an indicator of the presence of microorganisms. Furthermore, the increase in the band at ~1640 cm^{-1} and the new band formed at 1540 cm^{-1} were also noted in linen and cotton fibres degraded after two weeks in soil and attributed to proteins produced during microbial attack [49]. In biodegraded archaeological textiles, Kavkler et al. observed a downshift from 1430 cm^{-1} to 1420 cm^{-1} [57] of a contribution that is known to be sensitive to the cellulose lattice [60]. The shift, coupled with an increased intensity, was attributed to the presence of cellulose II [57], in line with Oh et al. [58]. In our yarns, both a shift and increased intensity were observed in

TS1 and TS2, but only in TS1 was severe biodegradation activity confirmed by AFM (Fig. 3c) and SHG (Fig. 6), where cavities and partial loss of fibre cells are visible. It should also be mentioned that the peak at 1420 cm^{-1} could be the contribution of the νC-O of calcium carbonate in calcite form [61].

The presence of a coating was observed in TS2 by SEM (Fig. 1L), and the high intensity of the amide bands at 1540 and 1644 cm^{-1} in its spectrum are indicative of a proteinaceous material, which supports the hypothesis of animal glue, probably from the glue paste.

The spectra of GB and NM are similar to that of the modern reference yarn, with the three bands at 1370, 1335 and 1315 cm^{-1}, sensitive to the cellulose lattice [60] clearly present, which are absent in TS1 and TS2. Furthermore, the bands between 1030 and 982 cm^{-1} merge in TS1 and TS2, while, in GB and NM, the peaks can still be distinguished despite a lower intensity than in the modern yarn. The same bands merged in a broad feature and were observed in naturally aged modern fabric [62]. At the same time, the decrease in the intensity of C-O vibrations between 1160 and 1030 cm^{-1} found in archaeological textiles was linked with cellulose hydrolysis [17]. In all four yarns from the canvases investigated in our work, a decrease in the intensity of these bands was noted.

Additionally, the band at 898 cm^{-1}, which is indicative of the cellulose structure [60], was observed to decrease in intensity in a biodegraded archaeological cotton fabric [57]. In GB and NM, this peak is still present but small and broad; in contrast, it is totally absent in TS1 and TS2.

In conclusion, FTIR-ATR observations allowed us to confirm the presence of animal glue in TS2 and highlight that TS1 underwent the greatest modifications in the cellulose structure. In contrast, yarns from GB and NM seem better preserved.

4.3.2 NMR results

The ^{13}CP-MAS spectrum can be considered a "fingerprint" of solid cellulose components, and all four canvases exhibit typical cellulose resonances (Fig. 5). The resonance at approximately 106 ppm is ascribed to anomeric carbon C1 of the glucose unit in cellulose and reveals the presence of two crystalline forms, namely, Iα and Iβ. The weak shoulder at approximately 102 ppm can be attributed to the anomeric carbon of hemicellulose polysaccharides [63].

In general, the cellulose matrix exhibits easily separable resonances from crystalline and less-ordered domains for the C4 and C6 atoms of the glucose unit. Resonances at 90.3 and 66.8 ppm labelled C4c and C6c are due to C4 and C6 of the crystalline phase, whereas those at 85.4 and 64.5 ppm labelled C4a and C6a are due to C4 and C6 of the amorphous phase.

Moreover, other resonances were also identifiable: in particular, the resonance at 30 ppm ascribable to CH_2 belonging to cutin, a waxy substance that covers cell walls, the resonances at 21 ppm and 18 ppm, ascribable to the acetyl and fucose groups of hemicellulose, respectively, and resonance at 177 ppm due to carboxyl groups of hemicellulose.

Figure. 5

In Table 4, the integrals (I) of resonances obtained from the deconvolution procedure of all spectra are reported together with the crystallinity index obtained from the ratio of the integrals C4c and (C4c+C4a).

The deconvolution of C1 resonance allowed us to obtain the amounts of I_α and I_β, the two allomorphs of cellulose. Our analysis showed that, in both modern and ancient flax yarns, the I_β allomorph was more abundant than the I_α allomorph. The ratio R between I_α and I_β depends on the origin of the cellulose [64]. Cellulose I_α is believed to be the dominant form in bacterial and algal celluloses, and cellulose I_β is the dominant form in higher plants, such as cotton ramie [65]. The R values for both modern and ancient flax yarns analysed in this study were found to be approximately 0.5–0.6, in accordance with the literature data on flax [66] and corresponding to the values that are usually assigned to non-lignified materials [67].

Table 4.

The normalised area of hemicellulose peaks at 20 and 30 ppm was found to be approximately 1.6% in modern flax, 2.4% in GB and 2.3% in TS1, while the area greatly increased in the case of canvases NM and TS2. In the case of NM, it could be probably due to a degradation process, while, in the case of canvas TS2, a change in the fingerprint of the resonances between 20–40 ppm was observed, which indicates the presence of another substance with resonances overlapping those of hemicellulose. In the same spectral region, there are resonances attributed to the protein of the animal glue. Thus, a hypothesis could be that animal glue is present on the flax fibres of yarn TS2, which was also confirmed by FTIR. The amount of carboxyl groups, which is approximately 0.8% in the modern flax, increased in canvases NM and TS2 and can be due to oxidation processes or, in the case of canvas TS2, to the presence of animal glue. Another result concerns the crystallinity index CI. The CI value obtained for canvases GB, NM, TS1 varied in a range between 53–58%, very similar to that found in modern flax (57% in Ref [62][68], 55% in this work), suggesting a good state of preservation for these

ancient yarns. A slight but significant decrease in crystallinity was observed in the TS2 canvas (see Table 4).

4.3.3 SHG results

The second harmonic is generated in the backward and forward directions, but a previous study showed that the forward direction is more suitable to investigating the network of cellulose microfibrils present in the cell walls of plant fibres [18], so we chose to use the latter one in the present work. The ultrastructure of flax fibres in yarns GB, NM and TS2 was well preserved and comparable to that of modern yarn (Fig. 6), with a visible cellulose macrofibril network [17,69], but some pits and other forms of degradation were occasionally observed as a result of oxidation and/or hydrolysis and a possible localised biological attack (Fig. A.4). In GB, traces of a different material were also found, which emitted a high-intensity second harmonic signal, as shown in Fig. 6 (white arrows), but the structure of the underlying fibres was intact, as highlighted by autofluorescence channels (Fig. A.3, white arrows). Since the foreign material generates a second harmonic but no fluorescence, this could suggest the presence of minerals or salts, as in the archaeological textiles studied previously [17]. The identification of this material is beyond the scope of this work.

Figure. 6

Concerning yarn TS2, despite the increased rigidity caused by glue-paste vitrification and the presence of some fractures into kink-bands, the cellulose microfibril network appeared intact under multiphoton microscopy.

All the ancient flax yarns presented sporadic degradation, identified with lacunae in the fibre structure, but yarn TS1 was in the worst state of preservation, and SHG analysis confirmed the AFM results: a severe biological attack was observed in the whole yarn. The fibre ultrastructure of this last sample was found to be highly degraded and compromised by cavities and lacunae, not only on the surface of the fibres but also into their inner structure down to the lumen.

5. Conclusions

Through this new combination of techniques, four Italian canvases dated between the 17th and 18th centuries have been investigated. The yarns extracted from each canvas were compared to a modern flax yarn to evaluate their state of preservation and highlight possible issues related to their chemical and mechanical conditions. Information on local mechanical properties obtained by nanoindentation and AFM helped to establish the state of preservation of cellulosic fibres, giving support and being complementary to chemical analyses such as FTIR and NMR. In addition, the SHG technique has proven to be fundamental to confirm the hypotheses of oxidation and biological attack formulated by the other techniques.

Yarn TS1 was found to be highly compromised by microorganisms, and future investigations should focus on assessing biological attack in the rest of the painting to avoid further degradation.

Despite the ageing, yarn GB appeared well preserved and comparable to the modern yarn. This could suggest that it was preserved in more favourable conditions before its acquisition and does not require immediate intervention.

Yarn NM showed some fibres with low mechanical properties recorded by AFM and nanoindentation, and the large amount of hemicellulose and carboxyl groups obtained by

NMR suggested the presence of an oxidation process. However, thanks to the SHG, it was noted that, in this sample, the fibre ultrastructure was mainly intact.

The fibre ultrastructure of yarn TS2 was generally preserved, as well as the mechanical properties that were comparable to those of the modern sample. On the other hand, the yarn of this last painting was the most brittle, and the increment in rigidity of the canvas due to the vitrification of the glue paste could be responsible for the lacunae and loss of the painting layer in the future. Furthermore, the re-lining process with glue paste could also trigger biodeterioration; however, in our case, we observed a rather limited number of fibres with signs of mould growth.

ACKNOWLEDGEMENTS

The authors would like to thank Dr. Stefano Papetti, director of the Civic Art Gallery in Ascoli, who granted us permission to sample the canvases and provided us with all needed information.

The authors would also like to thank the INTERREG IV Cross Channel programme for funding this work through the FLOWER project (Grant number n°23). The authors are also grateful to SOLEIL Synchrotron for funding the 99180266 in-house proposal.

REFERENCES

[1] W. Van Zeist, J.A.H. Bakker-Heeres, Evidence for linseed cultivation before 6000 bc, J. Archaeol. Sci. 2 (1975) 215–219. https://doi.org/10.1016/0305-4403(75)90059-X.

[2] C. Cennini, Di Cennino Cennini Trattato della pittura messo in luce la prima volta con annotazioni dal cavaliere Giuseppe Tambroni, Company' torchi di Paolo Salviucci, Rome, 1821.

[3] C. Giannini, Dizionario del restauro. Tecniche, diagnostica, conservazione, Nardini, Firenze, 2010, pp. 53, 97, 125

[4] S. Marconi, Preparazioni e Imprimiture dei dipinti su tavola e tela: materiali, metodi e storia, in: C. Maltese (Ed.), Preparazione e finitura delle opere pittoriche-materiali e metodi : preparazioni e imprimiture, leganti, vernici, cornici, Mursia, Milan, 1993: pp. 11–38.

[5] A.M. Seves, Aggressione microbica alle colle da rifodero, in: G.C. Scicolone (Ed.), Dipinti su Tela: metodologie d'indagine per i supporti cellulosici, 2nd edition, Nardini Editore, Firenze, 2005: pp. 41–44.

[6] S. Hackney, G. Hedley, Measurements of the Ageing of Linen Canvas, Stud. Conserv. 26 (1981) 1–14, https://doi.org/10.2307/1505816.

[7] C.R.T. Young, R.D. Hibberd, Biaxial Tensile Testing of Paintings on Canvas, Stud. Conserv. 44 (2) (1999) 129–141

[8] C.R.T. Young, R.D. Hibberd, The role of canvas attachments in the strain distribution and degradation of easel paintings, Stud. Conserv. 45 (sup1) (2000) 212–220, https://doi.org/10.1179/sic.2000.45.Supplement-1.212.

[9] P. Castellini, E. Esposito, B. Marchetti, N. Paone, E.P. Tomasini, New applications of scanning laser Doppler vibrometry (SLDV) to nondestructive diagnosis of artwork: mosaics, ceramics, inlaid wood, and easel painting, J. Cult. Herit. 4 (sup1) (2003), 321-329 https://doi.org/10.1016/S1296-2074(02)01148-2

[10] E. Rossi, Misure del grado di polimerizzazione per la valutazione dello stato di deterioramento di un materiale fibroso cellulosico, in: G.C. Scicolone (Ed.), Dipinti su

Tela: metodologie d'indagine per i supporti cellulosici, 2nd edition, Nardini Editore, Firenze, 2005: pp. 25–30.

[11] R.H. Newman, L.M. Davies, P.J. Harris, Solid-State 13C Nuclear Magnetic Resonance Characterization of Cellulose in the Cell Walls of Arabidopsis thaliana Leaves, Plant Physiol. 111 (2) (1996) 475–485, https://doi.org/10.1104/pp.111.2.475.

[12] P.T. Larsson, K. Wickholm, T. Iversen, A CP/MAS 13C NMR investigation of molecular ordering in celluloses, Carbohyd. Res. 302 (1-2) (1997) 19–25, https://doi.org/10.1016/S0008-6215(97)00130-4.

[13] L.K. Herrera, A. Justo, A. Duran, M.C.J. Haro, M.L. Franquelo, J.L. Perez Rodríguez, Identification of cellulose fibres belonging to Spanish cultural heritage using synchrotron high resolution X-ray diffraction, Appl. Phys. A. 99 (2) (2010) 391–398, https://doi.org/10.1007/s00339-010-5626-z.

[14] K. Kavkler, A. Demšar, Examination of cellulose textile fibres in historical objects by micro-Raman spectroscopy, Spectroc. Acta A 78 (2) (2011) 740–746, https://doi.org/10.1016/j.saa.2010.12.006.

[15] T. Cerchiara, G. Chidichimo, M.C. Gallucci, R. Ferraro, D. Vuono, A. Nastro, Use of Spanish broom (Spartium junceum L.) canvas as a painting support: Evaluation of the effects of environmental conditions, J. Cult. Herit. 10 (3) (2009) 396–402, https://doi.org/10.1016/j.culher.2008.12.002.

[16] O. Arnould, D. Siniscalco, A. Bourmaud, A. Le Duigou, C. Baley, Better insight into the nano-mechanical properties of flax fibre cell walls, Ind. Crop. Prod. 97 (2017) 224–228, https://doi.org/10.1016/j.indcrop.2016.12.020.

[17] C. Reynaud, M. Thoury, A. Dazzi, G. Latour, M. Scheel, J. Li, A. Thomas, C. Moulhérat, A. Didier, L. Bertrand, In-place molecular preservation of cellulose in

5,000-year-old archaeological textiles, PNAS. 117 (33) (2020) 19670–19676, https://doi.org/10.1073/pnas.2004139117.

[18] A. Melelli, F. Jamme, D. Legland, J. Beaugrand, A. Bourmaud, Microfibril angle of elementary flax fibres investigated with polarised second harmonic generation microscopy, Ind. Crop. Prod. 156 (2020), 112847, https://doi.org/10.1016/j.indcrop.2020.112847.

[19] N.H. Faisal, R. Ahmed, S. Goel, G. Cross, Future of nanoindentation in archaeometry, J. Mater. Res. 33 (2018) 2515–2532. https://doi.org/10.1557/jmr.2018.280.

[20] L. Han, X. Tian, T. Keplinger, H. Zhou, R. Li, K. Svedström, I. Burgert, Y. Yin, J. Guo, Even Visually Intact Cell Walls in Waterlogged Archaeological Wood Are Chemically Deteriorated and Mechanically Fragile: A Case of a 170 Year-Old Shipwreck, Molecules. 25 (2020) 1113. https://doi.org/10.3390/molecules25051113.

[21] ASTM C1557-20, Standard Test Method for Tensile Strength and Young's Modulus of Fibers, ASTM International, West Conshohocken, PA, 2020. https://doi.org/10.1520/C1557-20.

[22] G. Metz, X.L. Wu, S.O. Smith, Ramped-Amplitude Cross Polarization in Magic-Angle-Spinning NMR, J. Magn. Reson. 110 (2) (1994) 219–227, https://doi.org/10.1006/jmra.1994.1208.

[23] D. Massiot, F. Fayon, M. Capron, I. King, S.L. Calvé, B. Alonso, J.-O. Durand, B. Bujoli, Z. Gan, G. Hoatson, Modelling one- and two-dimensional solid-state NMR spectra, Magn. Reson. Chem. 40 (1) (2002) 70–76, https://doi.org/10.1002/mrc.984.

[24] L. Hammarlund, Handicraft Knowledge Applied to Archaeological Textiles, Nord. Text. J. (2005) 87–119.

[25] L. Fuster-López, C. Andersen, N. Bouillon, F. Fabien, M. Rossi-Doria, M. Scharff, K. Seymour, A. Vicente-Escuder, S. Vicente-Palomino, D. Yusà-Marco, Glue-paste linings: An evaluation of some biological, chemical and mechanical aspects of a traditional technique, in: Copenhagen, 2017.

[26] G. Vogeslang-Eastwood, Textiles, in: P.T. Nicholson, I. Shaw (Eds.), Ancient Egyptian Materials and Technology, Cambridge University Press, 2000: pp. 268–297.

[27] R.M. Kozłowski, M. Mackiewicz-Talarczyk, K. Wielgusz, M. Praczyk, A.M. Allam, Bast fibres: flax, in: Handbook of Natural Fibres, Woodhead Publishing, 2020: pp. 93–162. https://doi.org/10.1016/B978-0-12-818398-4.00006-2.

[28] E. Martuscelli, Degradazione delle fibre naturali e dei tessuti antichi : aspetti chimici, molecolari, strutturali e fenomenologici, Paideia, 2006, pp.90-91

[29] M. Aslan, G. Chinga-Carrasco, B.F. Sørensen, B. Madsen, Strength variability of single flax fibres, J. Mater. Sci. 46 (19) (2011) 6344–6354, https://doi.org/10.1007/s10853-011-5581-x.

[30] L.G. Thygesen, Quantification of dislocations in hemp fibers using acid hydrolysis and fiber segment length distributions, J. Mater. Sci. 43 (4) (2008) 1311–1317, https://doi.org/10.1007/s10853-007-2284-4.

[31] L.G. Thygesen, B.J. Hidayat, K.S. Johansen, C. Felby, Role of supramolecular cellulose structures in enzymatic hydrolysis of plant cell walls, J. Ind. Microbiol. Biotechnol. 38 (8) (2011) 975–983, https://doi.org/10.1007/s10295-010-0870-y.

[32] A.P. Singh, Y.S. Kim, T. Singh, Bacterial Degradation of Wood, in: Secondary Xylem Biology, Academic Press, 2016: pp. 169–190.

[33] P. Ackroyd, The structural conservation of canvas paintings: changes in attitude and practice since the early 1970s, Studies in Conservation. 47 (2002) 3–14. https://doi.org/10.1179/sic.2002.47.Supplement-1.3.

[34] K. Swerda, Painting conservation ideas, ethics,materials, and techniques in Nineteenth-century America, in: AIC PAINTINGS SPECIALTY GROUP POSTPRINTS, Arlington, Virginia, 2003: p. 40.

[35] J. Coddington, C. Young, Structure and Lining: A Review, AIC News. 43 (2018).

[36] C. Goudenhooft, D. Siniscalco, O. Arnould, A. Bourmaud, O. Sire, T. Gorshkova, C. Baley, Investigation of the Mechanical Properties of Flax Cell Walls during Plant Development: The Relation between Performance and Cell Wall Structure, Fibers. 6 (2018) 6. https://doi.org/10.3390/fib6010006.

[37] T.K. Bader, K. de Borst, K. Fackler, T. Ters, S. Braovac, A nano to macroscale study on structure-mechanics relationships of archaeological oak, J. Cult. Herit. 14 (5) (2013) 377–388, https://doi.org/10.1016/j.culher.2012.09.007.

[38] C. Goudenhooft, A. Bourmaud, C. Baley, Varietal selection of flax over time: Evolution of plant architecture related to influence on the mechanical properties of fibers, Ind. Crop. Prod. 97 (2017) 56–64. https://doi.org/10.1016/j.indcrop.2016.11.062.

[39] C. Baley, M. Gomina, J. Breard, A. Bourmaud, P. Davies, Variability of mechanical properties of flax fibres for composite reinforcement. A review, Ind. Crop. Prod. (2019) 111984. https://doi.org/10.1016/j.indcrop.2019.111984.

[40] V. Librando, Z. Minniti, S. Lorusso, Ancient and modern paper characterization by FTIR and Micro-Raman spectroscopy, CSCH. 11 (2011) 249–268. https://doi.org/10.6092/issn.1973-9494/2700.

[41] L. Pronti, M. Perino, M. Cursi, M.L. Santarelli, A.C. Felici, M.P. Bracciale, Characterization and Digital Restauration of XIV-XV Centuries Written Parchments by Means of Nondestructive Techniques: Three Case Studies, Journal of Spectroscopy. 2018 (2018) 1–14. https://doi.org/10.1155/2018/2081548.

[42] P. Garside, P. Wyeth, Identification of Cellulosic Fibres by FTIR Spectroscopy - Thread and Single Fibre Analysis by Attenuated Total Reflectance, Studies in Conservation. 48 (2003) 269–275. https://doi.org/10.1179/sic.2003.48.4.269.

[43] B.D. Lazić, B.M. Pejić, A.D. Kramar, M.M. Vukčević, K.R. Mihajlovski, J.D. Rusmirović, M.M. Kostić, Influence of hemicelluloses and lignin content on structure and sorption properties of flax fibers (Linum usitatissimum L.), Cellulose. 25 (2018) 697–709. https://doi.org/10.1007/s10570-017-1575-4.

[44] M. Zimniewska, W. Rozańska, A. Gryszczynska, B. Romanowska, A. Kicinska-Jakubowska, Antioxidant Potential of Hemp and Flax Fibers Depending on Their Chemical Composition, Molecules. 23 (2018) 1993. https://doi.org/10.3390/molecules23081993.

[45] M.C. Seghini, F. Touchard, F. Sarasini, L. Chocinski-Arnault, J. Tirillò, M.P. Bracciale, M. Zvonek, V. Cech, Effects of oxygen and tetravinylsilane plasma treatments on mechanical and interfacial properties of flax yarns in thermoset matrix composites, Cellulose. 27 (2020) 511–530. https://doi.org/10.1007/s10570-019-02785-3.

[46] A. Célino, S. Fréour, F. Jacquemin, P. Casari, Characterization and modeling of the moisture diffusion behaviour of natural fibres, J. Appl. Polym. Sci. 130 (2013) 297–306. https://doi.org/10.1002/app.39148.

[47] L. Hajji, A. Boukir, J. Assouik, A. Kerbal, M. Kajjout, P. Doumenq, M.L. De Carvalho, A Multi-Analytical Approach for the Evaluation of the Efficiency of the Conservation–

Restoration Treatment of Moroccan Historical Manuscripts Dating to the 16th, 17th, and 18th Centuries, Appl. Spectrosc. 69 (2015) 920–938. https://doi.org/10.1366/14-07688.

[48] C. Sendrea, C. Carsote, E. Badea, A. Adams, M. Niculescu, H. Iovu, Non-invasive characterisation of collagen-based materials by NMR-mouse and ATR-FTIR, Sci. Bull. B Chem. Mater. Sci. UPB. 78 (2016) 27–38.

[49] K. Arshad, M. Skrifvars, V. Vivod, J. Volmajer Valh, B. Vončina, Biodegradation of Natural Textile Materials in Soil, TEK. 57 (2014) 118–132. https://doi.org/10.14502/Tekstilec2014.57.118-132.

[50] H. Mohapatra, R. Malik, Effect of Microorganism on Flax and Linen, J Text. Sci Eng. 06 (2015). https://doi.org/10.4172/2165-8064.1000229.

[51] C. Margariti, The application of FTIR microspectroscopy in a non-invasive and non-destructive way to the study and conservation of mineralised excavated textiles, Herit Sci. 7 (2019) 63. https://doi.org/10.1186/s40494-019-0304-8.

[52] B. Zghari, L. Hajji, A. Boukir, Effect of Moist and Dry Heat Weathering Conditions on Cellulose Degradation of Historical Manuscripts exposed to Accelerated Ageing: 13C NMR and FTIR Spectroscopy as a non-Invasive Monitoring Approach, J. Mater. Environ. Sci. 9 (2) (2018) 641–654, https://doi.org/10.26872/jmes.2018.9.2.71.

[53] M. Zotti, A. Ferroni, P. Calvini, Microfungal biodeterioration of historic paper: Preliminary FTIR and microbiological analyses, Int. Biodeterior. Biodegradation 62 (2) (2008) 186–194, https://doi.org/10.1016/j.ibiod.2008.01.005.

[54] F. Kimura, J. Umemura, T. Takenaka, FTIR-ATR studies on Langmuir-Blodgett films of stearic acid with 1-9 monolayers, Langmuir. 2 (1986) 96–101. https://doi.org/10.1021/la00067a017.

[55] D. Pellegrini, C. Duce, I. Bonaduce, S. Biagi, L. Ghezzi, M.P. Colombini, M.R. Tinè, E. Bramanti, Fourier transform infrared spectroscopic study of rabbit glue/inorganic pigments mixtures in fresh and aged reference paint reconstructions, Microchem. J. 124 (2016) 31–35. https://doi.org/10.1016/j.microc.2015.07.018.

[56] M. Fan, D. Dai, B. Huang, Fourier Transform Infrared Spectroscopy for Natural Fibres, in: S. Salih (Ed.), Fourier Transform - Materials Analysis, InTech, 2012, pp.45-68. https://doi.org/10.5772/35482.

[57] K. Kavkler, N. Gunde-Cimerman, P. Zalar, A. Demšar, FTIR spectroscopy of biodegraded historical textiles, Polym. Degrad. Stabil. 96 (2011) 574–580. https://doi.org/10.1016/j.polymdegradstab.2010.12.016.

[58] S.Y. Oh, D.I. Yoo, Y. Shin, H.C. Kim, H.Y. Kim, Y.S. Chung, W.H. Park, J.H. Youk, Crystalline structure analysis of cellulose treated with sodium hydroxide and carbon dioxide by means of X-ray diffraction and FTIR spectroscopy, Carbohydr. Res. 340 (2005) 2376–2391. https://doi.org/10.1016/j.carres.2005.08.007.

[59] M. Cintrón, D. Hinchliffe, FT-IR Examination of the Development of Secondary Cell Wall in Cotton Fibers, Fibers. 3 (2015) 30–40. https://doi.org/10.3390/fib3010030.

[60] M.L. Nelson, R.T. O'Connor, Relation of certain infrared bands to cellulose crystallinity and crystal lattice type. Part II. A new infrared ratio for estimation of crystallinity in celluloses I and II, J. Appl. Polym. Sci. 8 (1964) 1325–1341. https://doi.org/10.1002/app.1964.070080323.

[61] B.H. Stuart, P.S. Thomas, M. Barrett, K. Head, Modelling clay materials used in artworks: an infrared spectroscopic investigation, Herit. Sci. 7 (2019) 86. https://doi.org/10.1186/s40494-019-0333-3.

[62] M. Ueland, J.M. Howes, S.L. Forbes, B.H. Stuart, Degradation patterns of natural and synthetic textiles on a soil surface during summer and winter seasons studied

using ATR-FTIR spectroscopy, Spectrochim. Acta A. 185 (2017) 69–76. https://doi.org/10.1016/j.saa.2017.05.044.

[63] A. Bourmaud, D. Siniscalco, L. Foucat, C. Goudenhooft, X. Falourd, B. Pontoire, O. Arnould, J. Beaugrand, C. Baley, Evolution of flax cell wall ultrastructure and mechanical properties during the retting step, Carbohydr. Polym. 206 (2019) 48–56. https://doi.org/10.1016/j.carbpol.2018.10.065.

[64] R.H. Atalla, D.L. VanderHart, Native Cellulose: A Composite of Two Distinct Crystalline Forms, Science. 223 (1984) 283–285. https://doi.org/10.1126/science.223.4633.283.

[65] B. Focher, M.T. Palma, M. Canetti, G. Torri, C. Cosentino, G. Gastaldi, Structural differences between non-wood plant celluloses: evidence from solid state NMR, vibrational spectroscopy and X-ray diffractometry, Ind. Crop. Prod. 13 (2001) 193–208. https://doi.org/10.1016/S0926-6690(00)00077-7.

[66] N. Ibragimova, N. Mokshina, M. Ageeva, O. Gurjanov, P. Mikshina, Rearrangement of the Cellulose-Enriched Cell Wall in Flax Phloem Fibers over the Course of the Gravitropic Reaction, Int. J. Mol. Sci. 21 (2020) 5322. https://doi.org/10.3390/ijms21155322.

[67] R.H. Atalla, D.L. Vanderhart, The role of solid state 13C NMR spectroscopy in studies of the nature of native celluloses, Solid State Nucl. Magn. Reson. 15 (1999) 1–19. https://doi.org/10.1016/s0926-2040(99)00042-9.

[68] N.E. Kotelnikova, E.F. Panarin, R. Serimaa, T. Paakkari, T.E. Sukhanova, A.V. Gribanov, Study of flax fibre structure by WAXS, IR and 13 C NMR spectroscopy, and SEM, in: Cellulosic Pulps, Fibres and Materials, Elsevier, 2000, pp. 169–179, https://doi.org/10.1533/9781845698546.169.

[69] A. Melelli, S. Durand, O. Arnould, E. Richely, S. Guessasma, F. Jamme, J. Beaugrand, A. Bourmaud, Extensive investigation of the ultrastructure of kink-bands in flax fibres, Ind. Crop. Prod. 164 (2021) 113368. https://doi.org/10.1016/j.indcrop.2021.113368.

TABLE CAPTIONS

Table 1. Dimensional and historical data on four canvases on display at the Civic Art Gallery of Ascoli Piceno.

Table 2. Summary of the techniques and parameters used.

Table 3. Summary of the bands considered in the FTIR analysis.

Table 4. Normalized integrals of resonance (in % of total area), crystallinity index CI (in %) and R ratio of cellulose crystalline forms obtained by applying the deconvolution procedure to ^{13}C CP-MAS spectra of modern flax and canvases GB, NM, TS1, TS2

FIGURE CAPTIONS

Figure. 1 Photos and macrographs of the different yarns (A,D,G,J - the weave count was measured over 4x4 cm^2) and SEM observations of yarns from canvas GB (B, C), NM (E, F), TS1 (H, I) and TS2 (J,K).

Figure. 2 Topography and indentation modulus maps of the surface of each yarn, as obtained by AFM in PF-QNM mode. Each profile corresponds to the red line indicated on the corresponding modulus map.

Figure. 3 a) Indentation modulus obtained by AFM and nanoindentation on the different samples, (b) hardness values measured by nanoindentation c) indentation modulus maps with fractures into the cell wall indicated by blue arrows; the white circle and zoom indicate traces of a possible biological attack near the lumen in the TS1 sample (lowered indentation modulus); the white arrow points to a fragment of a coating layer (preparation layer or re-lining intervention) in the TS2 sample (the interface with the cell wall is homogeneous, and the cell wall indentation modulus does not seem to be affected).

Figure. 4 a) FTIR spectra of canvases and modern flax yarn with a break in the region between 1890 and 2550 cm^{-1}; b) focus on three regions of interest.

Figure. 5 ^{13}C CP-MAS NMR spectra of canvas GB, NM, TS1 and TS2 and modern flax. On the spectrum of modern flax, a detailed assignment of the main resonances belonging to cellulose (in red) and to hemicellulose (in green) is given.

Figure. 6 Forward SHG images of the flax yarns. GB, NM and TS2 have a generally well-preserved ultrastructure with an intact cellulose network. White arrows indicate the presence of a foreign material in GB yarn (probably minerals or salts) and cavities/pits resulting from a severe biological attack in yarn TS1. Several kink-bands with a well-defined angle are found in TS2 (square inset), suggesting brittle behaviour.

Figure 1. Photos and macrographs of the different yarns (A,D,G,J - the weave count was measured over 4x4 cm^2) and SEM observations of yarns from canvas GB (B, C), NM (E, F), TS1 (H, I) and TS2 (J,K).

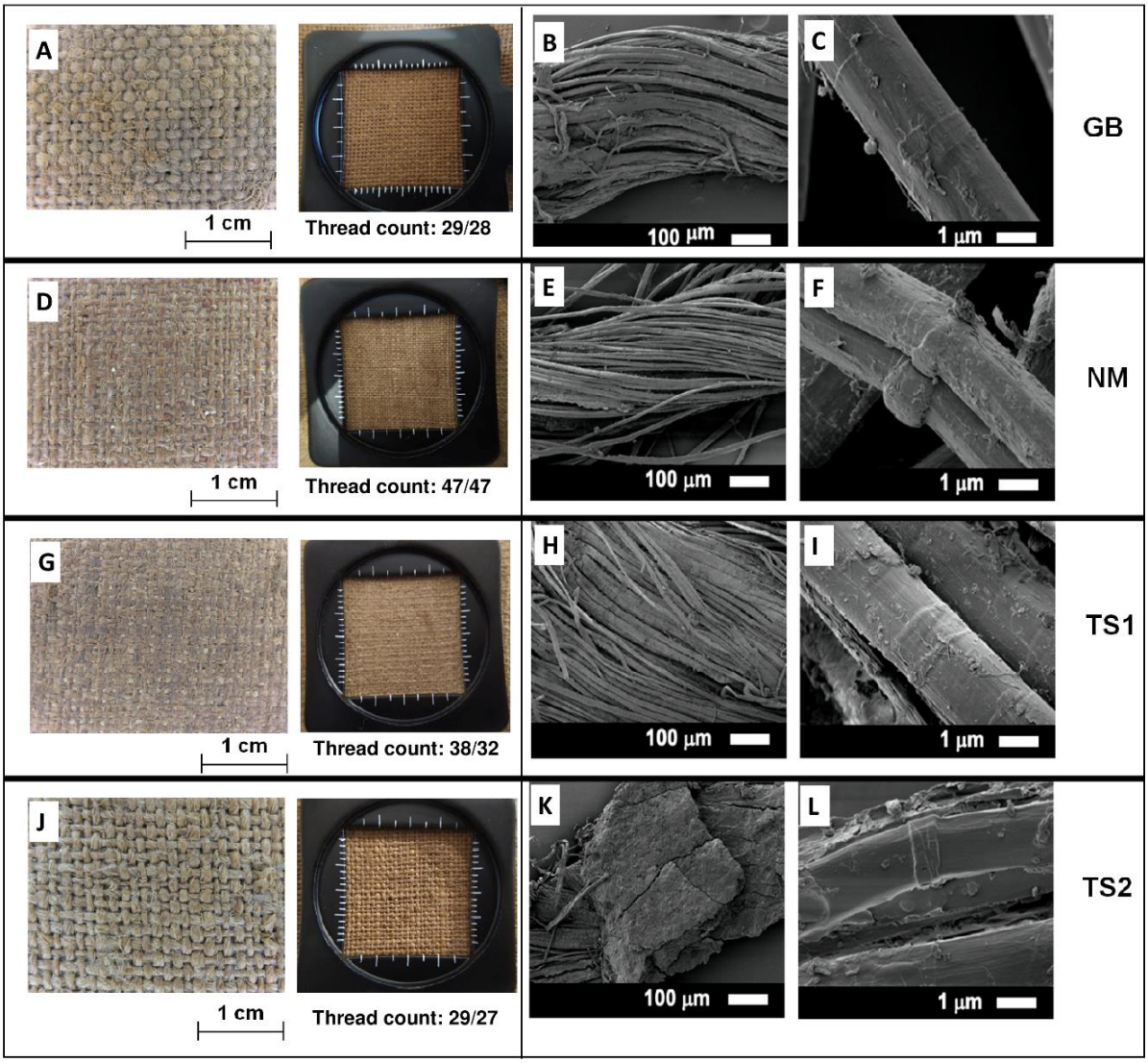

Figure 2. Topography and indentation modulus maps of the surface of each yarn, as obtained by AFM in PF-QNM mode. Each profile corresponds to the red line indicated on the corresponding modulus map.

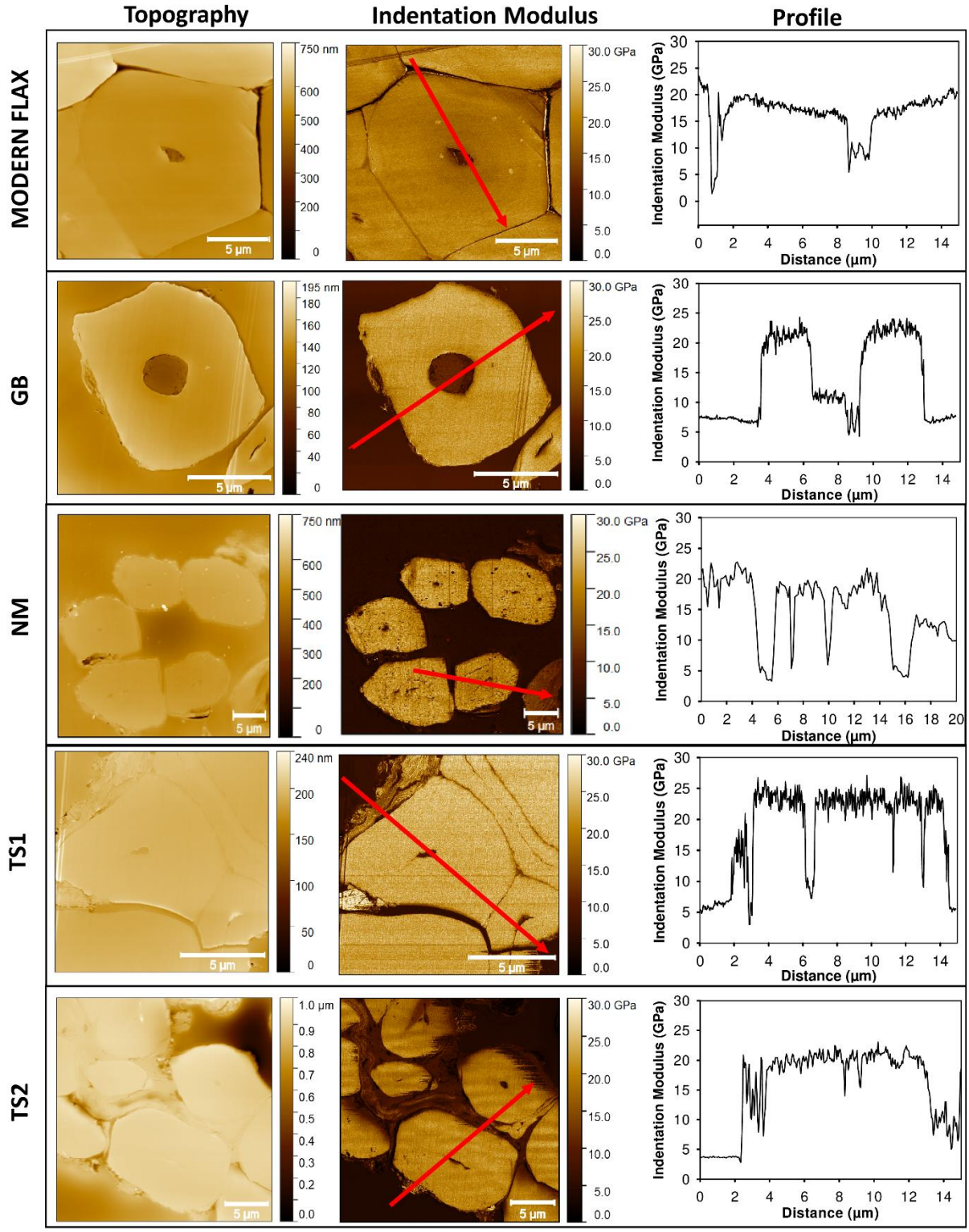

Figure 3. a) Indentation modulus obtained by AFM and nanoindentation on the different samples, (b) hardness values measured by nanoindentation c) indentation modulus maps with fractures into the cell wall indicated by blue arrows; the white circle and zoom indicate traces of a possible biological attack near the lumen in the TS1 sample (lowered indentation modulus); the white arrow points to a fragment of a coating layer (preparation layer or re-lining intervention) in the TS2 sample (the interface with the cell wall is homogeneous, and the cell wall indentation modulus does not seem to be affected).

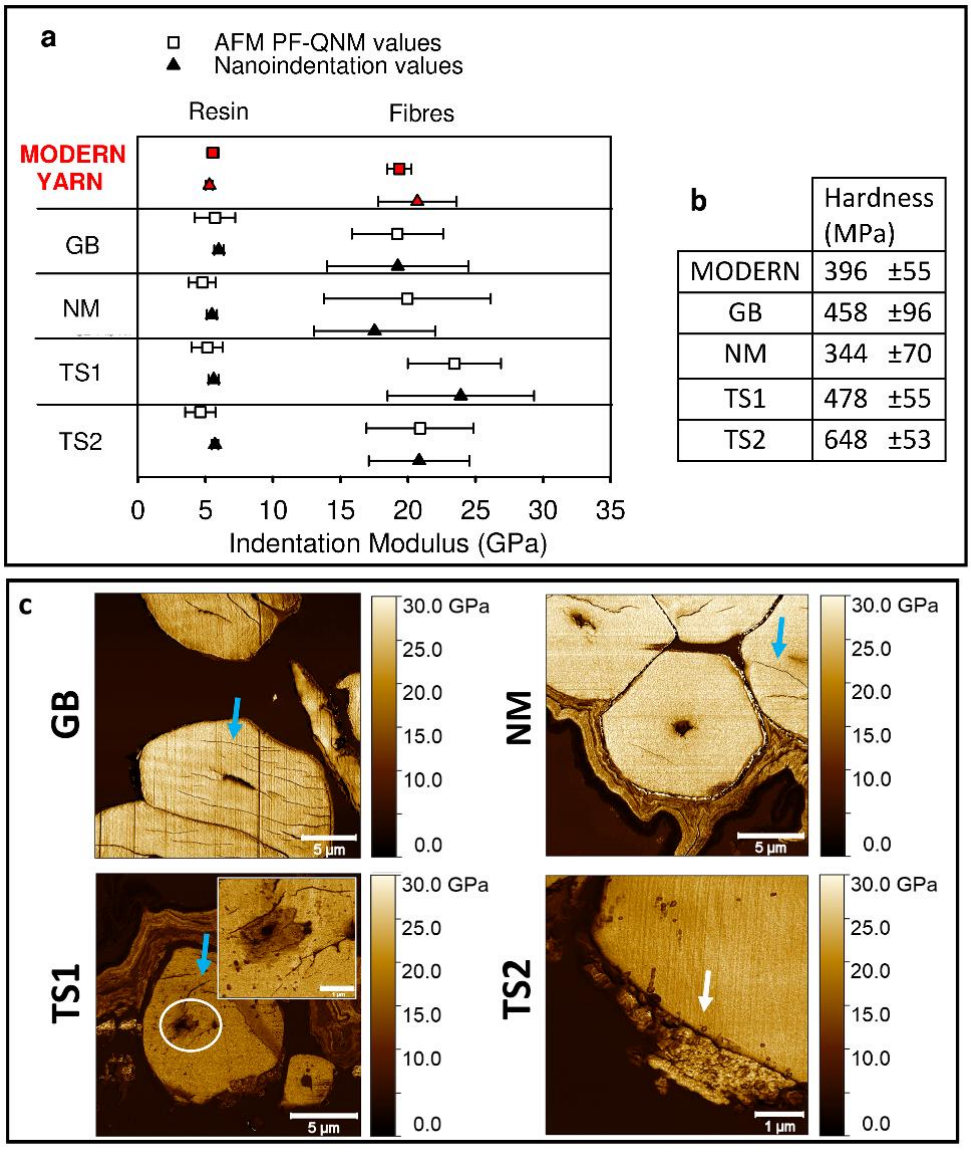

Figure 4. a) FTIR spectra of canvases and modern flax yarn with a break in the region between 1890 and 2550 cm^{-1}; b) focus on three regions of interest.

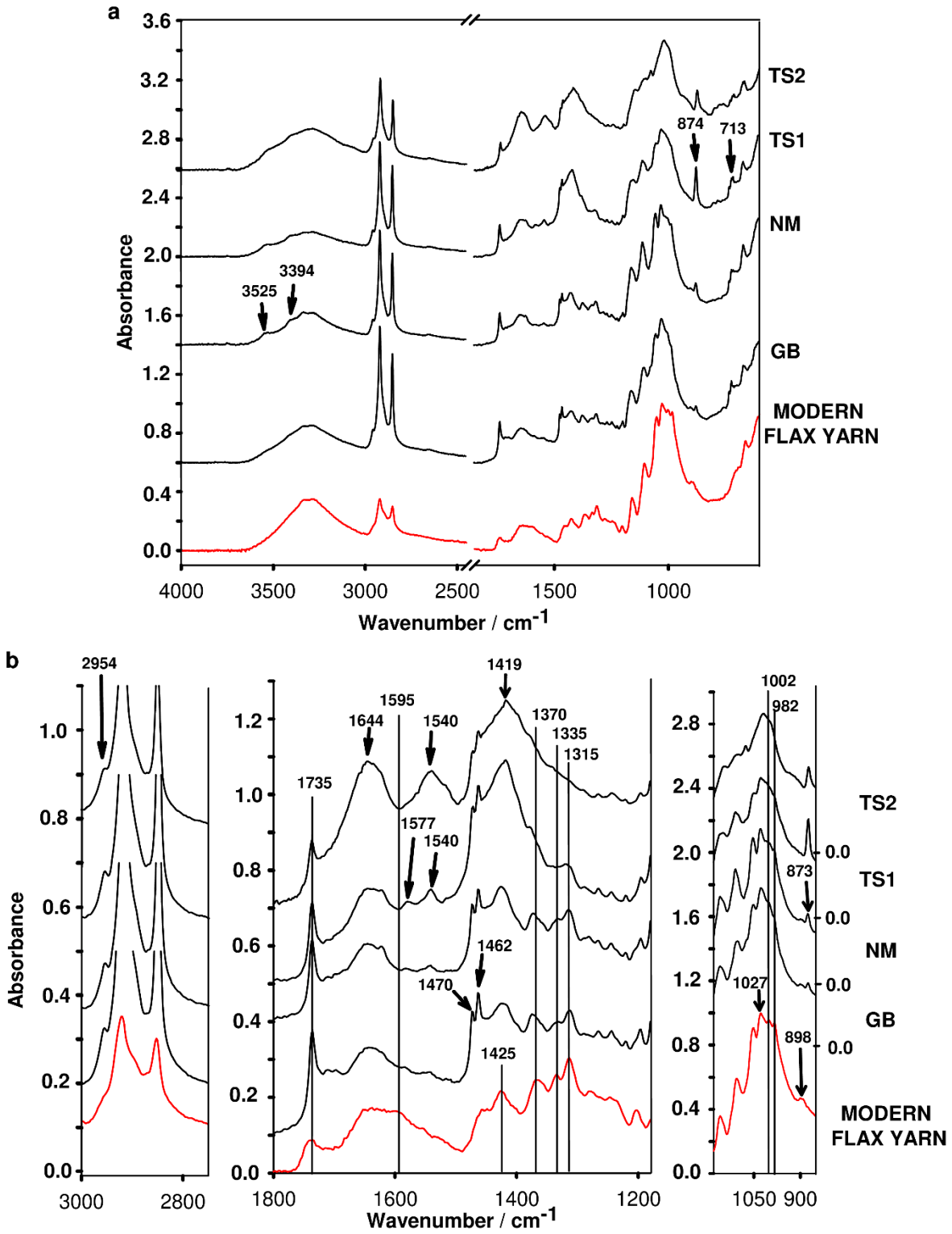

Figure 5. ^{13}C CP-MAS NMR spectra of canvas GB, NM, TS1 and TS2 and modern flax. On the spectrum of modern flax, a detailed assignment of the main resonances belonging to cellulose (in red) and to hemicellulose (in green) is given.

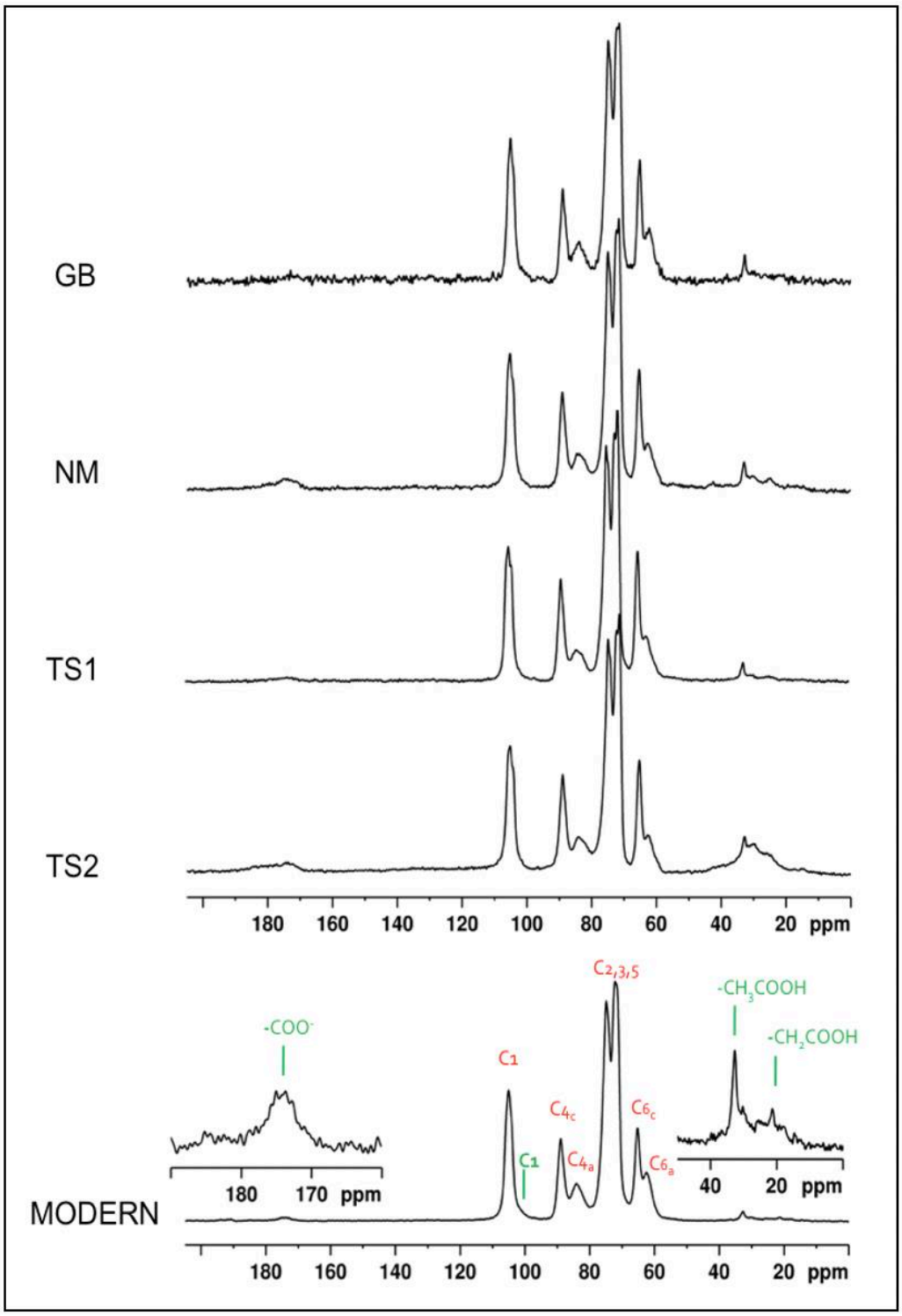

Figure 6. Forward SHG images of the flax yarns. GB, NM and TS2 have a generally well-preserved ultrastructure with an intact cellulose network. White arrows indicate the presence of a foreign material in GB yarn (probably minerals or salts) and cavities/pits resulting from a severe biological attack in yarn TS1. Several kink-bands with a well-defined angle are found in TS2 (square inset), suggesting brittle behaviour.

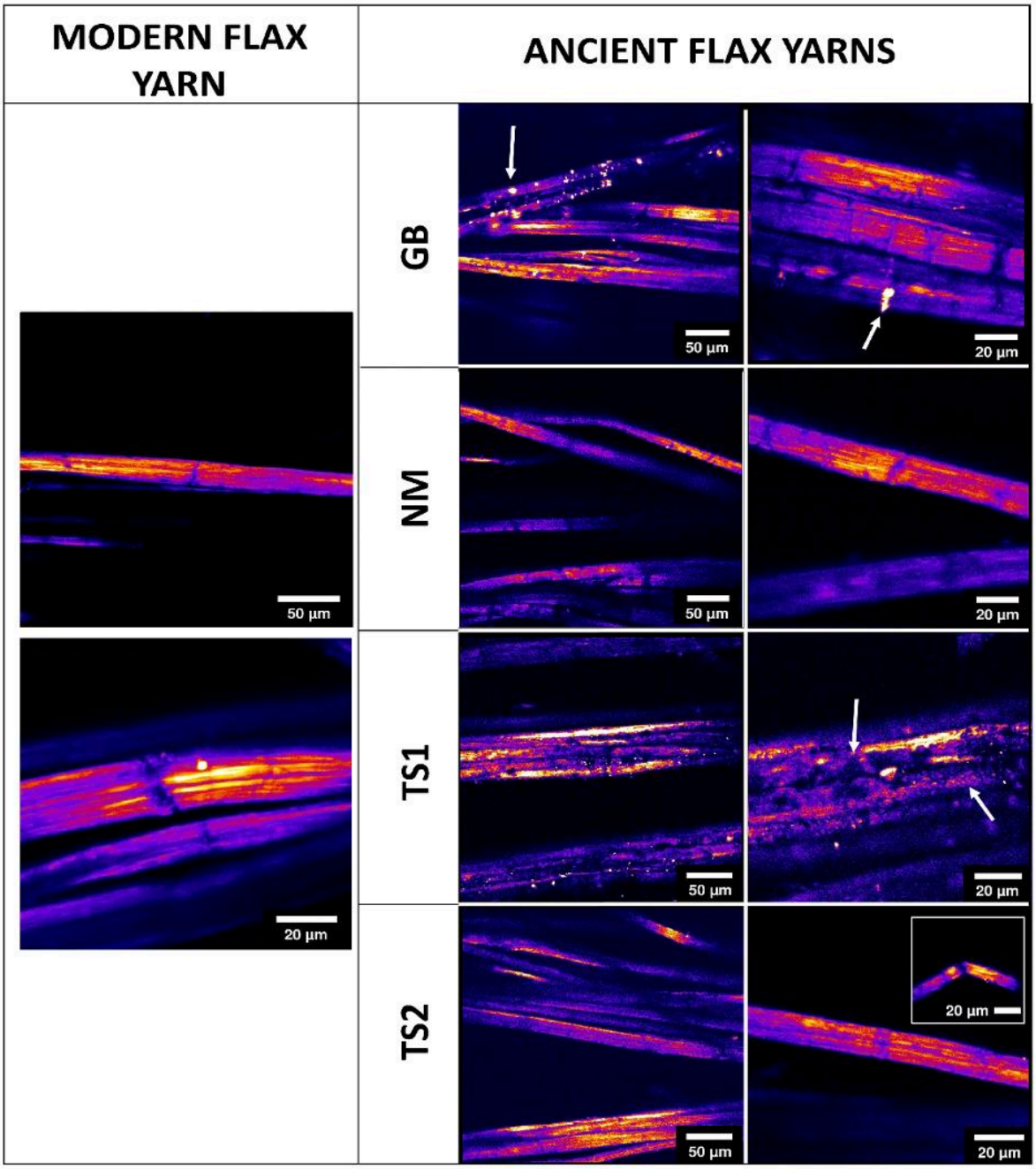

Table 1. Dimensional and historical data on four canvases on display at the Civic Art Gallery of Ascoli Piceno.

Sample	Author	Title and date	Origin	Dimensions (cm)	Picture
GB	Giulio Benso (1592–1668)	San Cristoforo (first half of the 17th century)	From the collection of Antonio Ceci; acquired by the Gallery in 1920	74x99	
NM	Nicola Monti (1736–1795)	Madonna col Bambino (18th century)	Commissioned for the Annunziata church (Ascoli Piceno) and exposed there until 1870, then acquired by the Gallery	100x72	
TS1	Tommaso Sciacca (1734–1795)	Crocefissione (18th century)	The two paintings were commissioned by the Camaldolese order of Sant'Angelo Magno convent (Ascoli Piceno) for the abbot's lodging and transferred into the Gallery in 1861. During the 19th century, Santa Francesca Romana painting (TS2) has undergone a re-lining intervention: a new canvas was glued to the back of the old one, which was in a bad state of preservation, to reinforce and support it	104x75	
TS2	Tommaso Sciacca (1734–1795)	Santa Francesca Romana (18th century)		64x46	

Table 2. Summary of the techniques and parameters used.

Characterization Technique	**Instrument**	**Parameters**
Scanning electron microscopy (SEM) EDX	Jeol JSM 6460LV scanning electron microscope	**Accelerating voltage:** 3 kV **Working distance:** 29.3–30.5 mm
Atomic Force Microscopy in Peak Force Nanomechanical property mapping mode (AFM PF-QNM)	Multimode 8 atomic force microscope (Bruker, USA) equipped with RTESPA-525 probes (Bruker, USA)	**Spring constant (Sader method):** 101–161 N/m **Deflection sensitivity:** calibrated on Sapphire **Tip radius (relative method on Aramid fibres):** 20–85 nm **Peak force setpoint**: 200 nN **Oscillation frequency**: 2 kHz **Resolution:** 512×512 pixels
Nanoindentation	Nanoindenter XP (MTS Nano Instruments)	**Indenter:** three-side pyramid indenter (Berkovich-Berko XPT-12761–0) **Surface approach velocity:** 10 nm/s **Frequency target:** 45 Hz **Loading rate:** 0.05 s^{-1} (i.e., 1 μN/s) **Unloading rate**: 10 μN/s **Depth limit:** 120 nm
Second Harmonic Generation Microscopic Imaging (SHG)	Multiphoton Nikon A1 MP+ microscope (NIKON, France) equipped with a long working distance (LWD) 16x (NA 0.80) water immersion objective (NIKON, France), a tuneable Mai Tai XF mode-5 locked Ti: sapphire femtosecond laser (SPECTRA PHYSICS, France) and a GaAsP NDD detector	**Excitation wavelength:** 810 nm (average power 1.5 W) **Laser power used:** 3% and 5% to investigate ancient and modern flax fibres, respectively to avoid bleaching **Bandpass filters**: 460/60 nm (autofluorescence), 550/88 nm (autofluorescence), 406/15 nm (SHG signal) **Scan line average:** 16 **Scan velocity**: 0.25 (fps) **Scan size:** 512×512 pixels
^{13}C CPMAS NMR	Bruker Advance III spectrometer operating at the proton frequency of 400.13 MHz	**Spin rate:** 12 KHz **Contact time for cross polarization:** 1.5 ms **Recycle delay:** 3 s **1H π/2 pulse width:** 3.5 μs
FTIR-ATR	Spectrum 100 Perkin-Elmer spectrophotometer equipped with ATR system with Zinc Selenium crystal (ZnSe)	**Accumulation scans :** 16 **Acquisition range** 4000–600 cm^{-1} **Resolution** : 4 cm^{-1}

Table 3. Summary of the bands considered in the FTIR analysis.

Assignment and position Wavenumber/cm^{-1}	Possible Attribution	MOD	GB	NM	TS1	TS2
~3525 and ~3394	νOH Gypsum ~~[35,36]~~ [40,41]	-	-	w	w	vw
3600–3100	νOH of free cellulose/ hemicellulose/lignin ~~[37,38]~~	sh	sh	sh	br	br
~2954	νCH_3 of lignin ~~[39]~~ [44]	-	w	w	w	vw
~1735	νC=O of carboxylic acid or esters groups of pectin and hemicellulose ~~[37,38]~~ [42,43]	w, br	m, sh	m, sh	m, sh	w, sh
~1635 or ~1644 (Amide I)	δOH of absorbed water ~~[40,41]~~ or νC=O (Amide I) of a protein binder ~~[42,43]~~ or produced by microorganisms ~~[44,45]~~ [45,46] [47,48] [49,50]	w, br	w, br	w, br	w, br	m, sh 1644 cm^{-1}
~1595	νC=C aromatic in plane of lignin ~~[37,46]~~ [42,51]	br	-	-	-	-
~1577	νC=O from oxidised phenolic lignin ~~[47]~~ [52] or νCOO^- of calcium stearate ~~[48,49]~~ with doublet at 1540 cm^{-1} [53,54]	-	vw	vw	w	-
~1540	νCOO^- of calcium stearate ~~[48,49]~~ or νC-N and δN-H in plane (Amide II) of protein binder ~~[42,43,50]~~ or produced by microorganisms ~~[44,45]~~ [47,48,55] [49,50] [53,54]	-	vw	vw	w, sh	m, sh
~1470	δCH_2 ~~[37,39]~~ [42,44]	-	sh	sh	sh	sh
~1462	δOH in plane ~~[37,41]~~ [42,46]	br	sh	sh	sh	sh
~1425	δO-C-H and δH-C-H in plane ~~[16,51–53]~~ [17,56-58]	m	m	m	s 1419 cm^{-1}	s 1419 cm^{-1}
~1375	δC-H and δCOH of cellulose, hemicellulose [17,57,59]	m	m	m	-	-
~1335	δCH_2 and δCOH mainly cellulose [17,42,51,58]	w, sh	w, br	w, br	-	-
~1315	δCH_2 wagging and δCOH of cellulose, hemicellulose ~~[16,41,53]~~ [17,46,58]	m, sh	m, sh	m, sh	w, br	-
~1027	νC-O ~~[16,46]~~ [17,51]	s, sh	s,sh	s,sh	s, br	s, br, 1019 cm^{-1}
~1002	νC-O ~~[16,54]~~ [17,59]	w, sh	-	vw, br	-	-
~982	νC-O ~~[16,53]~~ [17,58]	sh	-	br	-	-
~898	νC-O-C of β-Glycosidic bond ~~[37,46,52]~~ [42,51,57]	w	vw	vw	-	-
~874 and ~713	Calcite [52]	-	w	s	s	s

s= strong; m= medium; w=weak; vw= very weak; sh=sharp; br=broad

Table 4. Normalised integrals of resonance (in % of total area), crystallinity index CI (in %) and R ratio of cellulose crystalline forms obtained by applying the deconvolution procedure to ^{13}C CP-MAS spectra of modern flax and canvases GB, NM, TS1, TS2

Sample	***I (I_α)***	***I (I_β)***	***I (C4c)***	***I (C4a)***	***I (Hemicellulose)***	***I (COO-)***	***CI***	***R= I_α/I_β***
modern flax	5.1	9.2	8.5	6.1	1.6	0.8	57	0.55
GB	5.3	9.2	8.2	6.6	2.4	n.d.	55	0.58
NM	4.7	8.6	8.5	5.8	4.7	2.8	59	0.55
TS1	5.0	9.4	9.2	6.1	2.3	0.7	60	0.53
TS2	4.2	8.4	7.6	7.3	7.7	3.2	51	0.50